Fracture of dual crosslink gels with permanent and transient crosslinks: Effect of the relaxation time of the transient crosslinks

Jingwen Zhao, Louis Debertrand, Tetsuharu Narita, Costantino Creton

Journal of Rheology 66, 1255 (2022); doi: 10.1122/8.0000460

Fracture of dual crosslink gels with permanent and transient Crosslinks – effect of the relaxation time of the transient crosslinks

Jingwen Zhao[1], Louis Debertrand[1], Tetsuharu Narita[1,2]* and Costantino Creton[1,2]*

[1] Laboratoire Sciences et Ingénierie de la Matière Molle, ESPCI Paris, PSL University, Sorbonne Université, CNRS, F-75005 Paris, France.

[2] Global Station for Soft Matter, Global Institution for Collaborative Research and Education, Hokkaido University, Sapporo, Japan

Email: costantino.creton@espci.psl.eu

Abstract

We investigate the fracture properties of poly(acrylamide-co-1-vinylimidazole) dual crosslink hydrogels (P(AAm-co-VIm)-M^{2+} gels) containing a small fraction of covalent bonds and a majority of dynamic bonds based on metal coordination bonds (Ni^{2+} or Zn^{2+}). Unlike a previous study on a different dual crosslink hydrogel system having slower dynamic bonds based on poly(vinylalcohol) and borate ions (PVA-Borax gels), the presence of these faster dynamic coordination bonds has two main effects: They significantly toughen the P(AAm-co-VIm)-M^{2+} gels even at high stretch rates, where the dynamic bonds should in principle behave as covalent bonds at the crack tip, and they toughen the gels at very low stretch rates, where the dynamic bonds are invisible during the loading stage. We propose two additional molecular mechanisms to rationalize this behavior of P(AAm-co-VIm)-M^{2+} gels: we hypothesize that fast exchanging dynamic bonds remain slow compared to the characteristic time of bond scission and are therefore able to share the load upon covalent bond scission even at low loading rates. We also argue of the existence of longer-lived clusters of dynamic bonds that introduce a stretch rate dependent strain hardening in uniaxial tension and stabilize and increase the size of the dissipative zone at the crack tip, thereby introducing a strain dependent dissipative mechanism.

1. Introduction

Hydrogels, initially an object of academic curiosity[1], find increasing applications in the biomedical field where their combination of hydrophilicity, drug release capability and biocompatibility makes them ideal in biological environments[2-3]. Initially believed to be brittle, hydrogels were first studied for their swelling properties as sophisticated sponges[4]. However more recently the combination of deformability and swelling ability[5] and the mechanical strength[6-12] became the focus of much academic attention pioneered by the works of Gong[6] and Suo[8]. In particular recent advances in materials chemistry have led to the discovery of a variety of gels with truly remarkable properties, designed with a more sophisticated crosslinking structure or a more complex composition[6, 8, 13-17] . The diversity of synthetic approaches designed to boost the strength of the hydrogel is large but can often be reduced to the description given by Zhao of "introducing dissipation in a stretchy network"[18].

It is not our purpose here to review extensively the literature on tough gels but to focus on a specific type of gel design principle: the dual crosslink gels, where the same hydrophilic polymer chains are crosslinked by dynamic bonds and by permanent crosslinks[19-23]. In order to obtain toughness, the stretchability of the gel requires a higher density of dynamic bonds relative to fixed crosslinks. Although engineering wise many gels of that type have been developed with remarkable properties[24-27] it is still not yet possible to predict fracture energy from simple molecular design for these dynamic bond systems. One of the reasons is the complexity of the exchange reactions that can involve multiple equilibriums and are generally simplified in current models. Theoretically a dynamic bond has simply one exchange time[21-22, 28] and is randomly dispersed; however, in reality things can be more complex.

In previous studies, we investigated in detail a simple model system of dual crosslink hydrogels made by a very simple synthetic route. Starting from a loosely crosslinked chemical network

of poly(vinyl alcohol) (crosslinked by glutaraldehyde), a PVA-borax dual crosslink gel was prepared by incorporating borate ions to form dynamic covalent bonds used as transient bonds[19-23, 29-31]. The PVA-borax dual crosslink gels exhibit clear time-dependent elasticity and a well-defined averaged relaxation time determined from a peak in $G''(\omega)$. We characterized the mechanical properties of the gel as a function of stretch rate, and demonstrated some unique rheological features, such as additivity of the contribution of the permanent and transient crosslinks to the viscoelastic moduli[20, 23], and, in large strain tests, the separability of the uniaxial tensile stress into a time-dependent and a strain-dependent contribution.[19] A constitutive model was developed that was able to describe both tensile and shear behaviors of the time and strain dependent stress with only four physically based parameters[21-22, 29].

While, in principle, the dynamics of such dual crosslink gels can be studied as a function of the relaxation time of the network (related to the bond dissociation time)[32], doing so in the PVA-borax system proved to be difficult. Therefore, we designed another dual crosslink hydrogel based on polyacrylamide, transiently crosslinked by metal-ligand coordination bonds. The chemical gel of the poly(acrylamide-*co*-1-vinylimidazole), P(AAm-co-VIm), possesses imidazole ligands, which can be transiently crosslinked by metal ions, Ni^{2+} or Zn^{2+} [33]. In small amplitude shear measurements[33], the P(AAm-*co*-VIm)-Zn^{2+} dual crosslink gel, has much faster association/dissociation dynamics than the P(AAm-*co*-VIm)-Ni^{2+} dual crosslink gel and at accessible stretch rates of 0.06 s^{-1} the P(AAm-*co*-VIm)-Zn^{2+} exhibits a lower hysteresis in tensile loops at intermediate stretch ($\lambda < 2$)[33]. Furthermore, a separability of the stress into strain-dependent and time-dependent terms was also confirmed. At larger strains, the stretch at break of the dual crosslink gels are much higher than that of the chemical gel even at stretch rates significantly lower than the inverse of the main relaxation time of the gel, a regime where the stress-strain curves of chemical and dual crosslink gels are nearly identical except for the fracture point.

In our two previous publications[33-34] we investigated the small and large strain mechanical properties of these dual crosslink gels establishing the relation between macroscopic viscoelasticity and reversible dissociation of the transient bonds. Here we focus on macroscopic fracture mechanisms of the same hydrogels.

Similar systematic fracture tests were carried out on the PVA-borax dual crosslink hydrogel[9] and showed clearly an increasingly brittle behavior with increasing strain rate, justified by the fact that dynamic bonds are no longer dynamic at sufficiently high strain rates, and hence the material simply behaves as a more chemically crosslinked gel. Yet at very low strain rate when all dynamic bonds freely exchange, the dual crosslink gel was still found to be significantly tougher than the pure chemical gel in contradiction to expectations. A recent theoretical paper of Tito et al.[35] introduced the idea that dynamic bonds may exchange at a rate that is fast compared to the loading rate, but slow relative to the actual molecular fracture process, so that dynamic bonds can protect the material from force transfer from one covalent bond to the next and delay nucleation of cracks. Furthermore, they argued that the weak dynamic bonds could form, for entropic reasons, clusters.

To investigate whether the fracture behavior of dual crosslink gels is universal, we report here a systematic study on fracture properties of P(AAm-*co*-VIm)-M^{2+} dual crosslink hydrogels. Effects of the ion species and stretch rate on the fracture mechanics of the single edge notch dual crosslink gels will be shown. Fracture energy of the dual crosslink gels are estimated by taking account of the time dependent dissipative nature of the gels, with the method that we have previously proposed to interpret the fracture behavior of PVA-borax dual crosslink gels. Thus comparison with the PVA-borax gel will be also discussed, considering the difference of the transient bond dynamics of these dual crosslink gels.

2. Experimental section

2.1 Materials

Acrylamide (AAm), 1-vinylimidazole (VIm), *N*,*N*'-methylene bisacrylamide (MBA), potassium persulfate (KPS), *N*,*N*,*N*',*N*'-Tetramethylethylenediamine (TEMED), nickel chloride and zinc chloride were purchased from Sigma Aldrich. Sodium chloride was purchased from Fluka. All the chemicals were used as received. Milli-Q water was used for the sample preparation.

2.2 Sample Preparation

Chemical and dual crosslink gel preparation procedure was previously described[34] in detail. Briefly, chemical gels polymerized from AAm and VIm were prepared by mixing AAm (1.8 M) and VIm (0.2 M) in aqueous solution with MBA (3 mM, 0.15 mol% relative to monomer concentration, 2 M) and KPS (6 mM), under nitrogen flow at low temperature (in ice bath). The solution was then transferred in a glovebox and TEMED (20 mM) was added. After the overnight crosslinking reaction, the resulting P(AAm-*co*-VIm) chemical gels were used for measurements as prepared. P(AAm-*co*-VIm)-M^{2+} dual crosslink gels were prepared by adding 0.1 M of $NiCl_2$ or $ZnCl_2$ in the reaction solution priori to polymerization. After the overnight crosslinking reaction, the resulting P(AAm-*co*-VIm)-Ni^{2+} or P(AAm-*co*-VIm)-Zn^{2+} dual crosslink gels were used for mechanical measurements as prepared. The structure of the P(AAm-*co*-VIm)-M^{2+} dual crosslink gel is schematically shown in **Figure 1**.

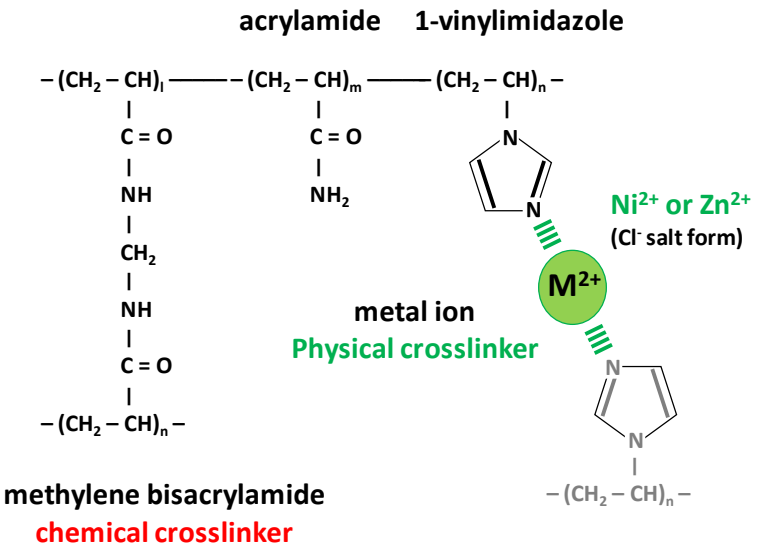

Figure 1 Schematic of the chemical structure of P(AAm-*co*-VIm)-M^{2+} dual crosslink hydrogel.

2.3 Experimental setup and sample geometry

Mechanical and fracture properties of the P(AAm-*co*-VIm)-M^{2+} dual crosslink gels were studied by uniaxial tensile tests with un-notched and notched samples of the gels. An Instron 5565 tensile tester with a 10 N load cell was used. Un-notched and notched samples were rectangular with a width of w = 10 mm, thickness of 1.5 mm, and length of 20 mm (length between clamps) (**Figure 2a**). A notch of approximately c = 2 mm was made with a scalpel, the actual length of the initial crack was measured for each sample from pictures of the sample with a ruler using ImageJ. The sample was then fixed in the clamps. To prevent slip in the clamp, pieces of sandpaper were glued to the clamp surfaces in contact with the gel samples. We kept the samples in paraffin oil during all the tests to prevent them from drying. The value of stretch λ was calculated from the cross-head displacement that moved at a constant velocity. The measured force, normalized by the initial cross-section of the sample is used to define the engineering stress. A camera (SENTECH STC-MBCM) was used to record the crack propagation process. **Figure 2b** shows an example of the experimental setup, with the chemical gel between the clamps.

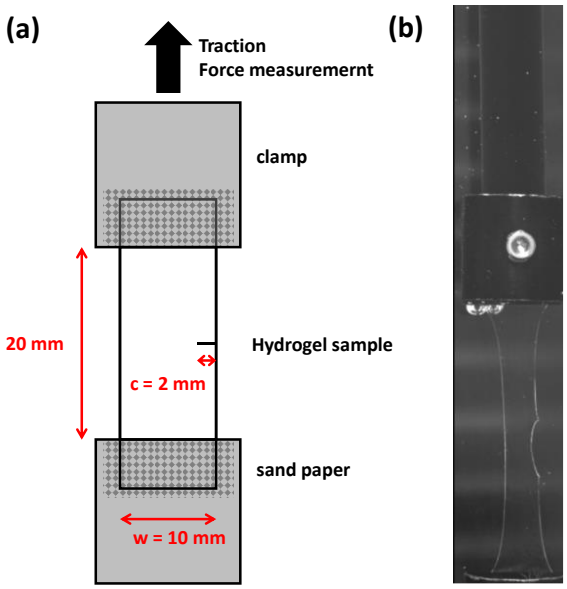

Figure 2. (a) Schematic view of sample geometry for single edge notch tests (unstretched). (b) Fracture tests setup, with a notched chemical gel sample (stretched).

The linear viscoelastic properties of the dual crosslink gels were characterized by small strain oscillatory shear rheometry. The ARES LS1 rheometer (TA instruments) with parallel plates geometry having roughened surfaces (20 mm in diameter) was used. The sample thickness was 1.5 mm. Frequency sweep tests with a dynamic range varying from 0.1 to 100 rad/s were carried out at 5, 15 and 25 °C within the linear viscoelasticity regime (0.2 – 0.8 % strain).

3. Results and discussion

3.1 Linear and nonlinear properties of the unnotched dual crosslink gels

The dynamics of the transient crosslinks and the relaxation time of the P(AAm-*co*-VIm)-M^{2+} dual crosslink gels can be tuned by changing the species of the transient metal ions. Here, we used Ni^{2+} and Zn^{2+} that have different metal-ligand coordination dynamics to study the fracture properties of the hydrogels. **Figure 3(a)** shows the dynamic moduli of the two dual crosslink gels with Ni^{2+} and Zn^{2+} and those of the corresponding chemical gel as a function of frequency. The sparsely crosslinked chemical gel has a weakly frequency dependent $G' \sim 1$ kPa and tan δ values 0.1 – 0.35. Both P(AAm-*co*-VIm)-Ni^{2+} and P(AAm-*co*-VIm)-Zn^{2+} dual crosslink gels exhibit a viscoelastic behavior, with an elastic modulus G' higher than G'' over the whole frequency range and values of the moduli higher than those of the chemical gel, since the physical and chemical crosslinks contribute to the moduli additively[20]. Our simple physical picture of the dual crosslink gels implies that the modulus of the dual crosslink gel at sufficiently low frequency should be equal to that of the corresponding chemical gel, due to the exchange of transient crosslinks[19-20]. Yet **Figure 3(a)** shows clearly that even at the lowest value of ω, corresponding to frequency much lower than the inverse of the main relaxation time of the gels, G' remains higher than that of the chemical gel. This result suggests that there exists a slower relaxation mode in the dual crosslink gel and that a small fraction of the transient bonds does not dissociate over the time scale of the stretch rates studied here.

For the P(AAm-*co*-VIm)-Ni^{2+} gel, G' continues to increase with increase in frequency, while G'' exhibits a peak, indicating that transient imidazole–Ni^{2+} coordination bonds dissociate and the network relaxation occurs. We define the network relaxation time τ_R from this peak (τ_R = 0.022 s for P(AAm-*co*-VIm)-Ni^{2+} gel). For the P(AAm-*co*-VIm)-Zn^{2+} gel, however, both moduli continue to increase and no peak of G'' is observed in the studied frequency range. This

result indicates that the imidazole–Zn^{2+} bonds dissociate faster than the imidazole–Ni^{2+} bonds. In order to estimate the relaxation time of the P(AAm-*co*-VIm)-Zn^{2+} gel, we construct a master curve of the loss tangent tan δ, by assuming that the network relaxation of the two gels is governed by the same dynamics driven by transient bonds having different dissociation rates [36]. In Figure 3(b) we show a master curve of tan δ vs shifted ω for the two hydrogels at three different temperatures. The master curve is constructed in two steps. First, for each gel, a master curve is obtained at a reference temperature of 25 °C by using the time-temperature superposition principle. Then the master curve of the P(AAm-*co*-VIm)-Ni^{2+} gel is further horizontally shifted to obtain a universal transient bond master curve. From the universal master curve made with a horizontal shift factor of about 1100, the relaxation time τ_R of the P(AAm-*co*-VIm)-Zn^{2+} gel can be estimated to be 0.020 ms. Note that for various ligands, the rate constant for ligand (solvent) exchange is typically about 1000 times faster for Zn^{2+} than for Ni^{2+} [37] and our rough estimate of the Zn^{2+} gel relaxation time from the universal master curve is consistent with that figure.

Additionally, from each individual master curves obtained by time-temperature superposition, we can determine the activation energy of bond dissociation using an Arrhenius plot of the horizontal shift factor, as shown in the inset of Figure 3(b). We found 79 kJ/mol for Ni^{2+} and 68 kJ/mol for Zn^{2+}. These values are close to the values found in the literature for monomeric imidazole (about 80 and 70 kJ/mol).[38]

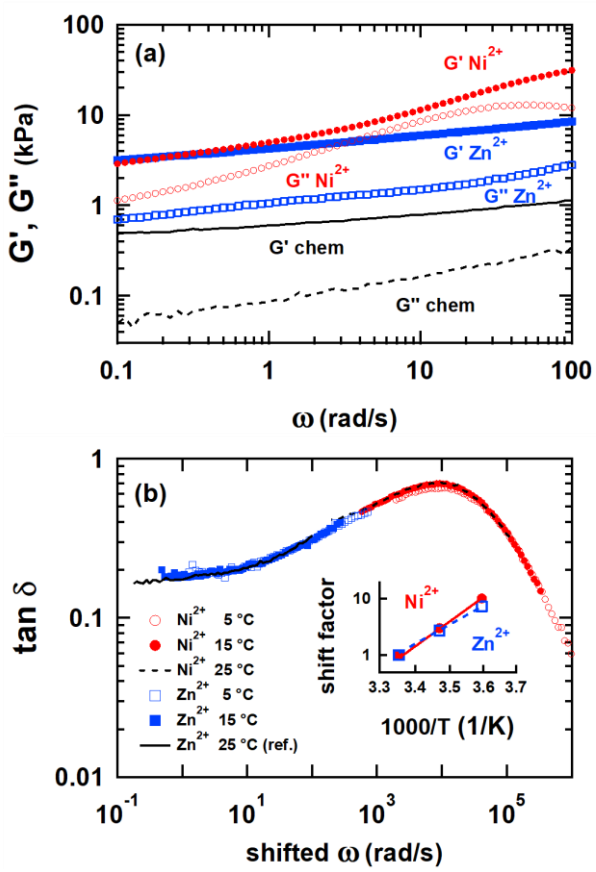

Figure 3 (a) Small amplitude oscillaroty shear measurements of P(AAm-*co*-VIm)-M^{2+} dual crosslink gels and the corresponding chemical gel at 25 °C. Filled symbols and solid line: *G*'; open symbols and dashed line: *G*". Red circles; P(AAm-*co*-VIm)-Ni^{2+} dual crosslink gel; blue squares: P(AAm-*co*-VIm)-Zn^{2+} dual crosslink gel; black lines: chemical gel. (b) Universal master curve of tan δ (ω) as a function of shifted frequency for P(AAm-*co*-VIm)-M^{2+} dual crosslink gels. The reference: P(AAm-*co*-VIm)-Zn^{2+} dual crosslink gel at 25 °C. Inset: Arrhenius plot of horizontal shift factors for P(AAm-*co*-VIm)-M^{2+} dual crosslink gels (color online).

In order to characterize the large stretch behavior of P(AAm-*co*-VIm)-M^{2+} dual crosslink gels and of the corresponding chemical gel, uniaxial tensile tests were carried out with *unnotched* samples at different constant crosshead velocities (and hence at constant stretch rates $\dot{\lambda}$) and are shown in **Figure 4**. The soft and brittle chemical gel ruptures at a critical stretch $\lambda_C \sim 3.5$ at a stress lower than 10 kPa and does not exhibit any particular stretch rate dependence (data not shown). Compared to the chemical gel, both P(AAm-*co*-VIm)-Ni^{2+} and P(AAm-*co*-VIm)-Zn^{2+} dual crosslink gels exhibit:

(1) a higher initial modulus at all stretch rates, consistent with the linear rheology results of **Figure 3**, (2) a higher stretch at break, with $\lambda_C > 6$ for the Ni^{2+} gel and $\lambda_C > 9$ for the Zn^{2+} gel, (3) a softening then hardening behavior with increasing stretch, and (4) a strong stretch rate dependence, as shown in **Figure 4(a)**. Remarkably for both gels at low stretch rates, the values of the stress are close to that of the chemical gel but the extensibility is still significantly improved.

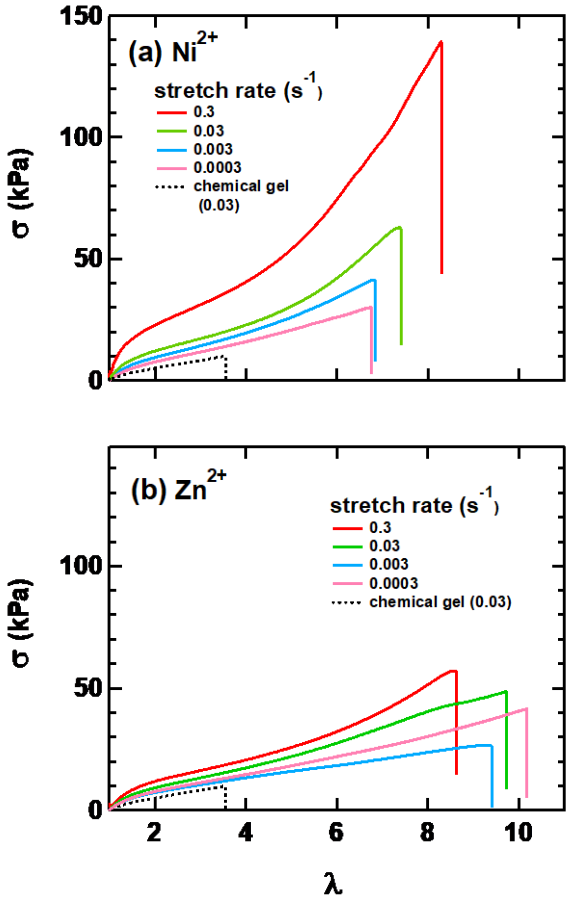

Figure 4 Stress – stretch curves of the unnotched P(AAm-*co*-VIm)-M^{2+} dual crosslink gels and of the chemical gel at different stretch rates. (a) P(AAm-*co*-VIm)-Ni^{2+} dual crosslink gel, (b) P(AAm-*co*-VIm)-Zn^{2+} dual crosslink gel.

3.2 Fracture: Uniaxial tension tests on notched dual crosslink gels

In order to characterize the fracture energy of the gels, uniaxial tensile tests were performed with single edge notch samples of P(AAm-*co*-VIm)-M^{2+} dual crosslink gels, compared with the corresponding chemical gel. **Figure 5** shows the stress – stretch curves of these *notched* samples

at $\dot{\lambda}$ varying from 0.3 to 0.0003 s^{-1}. The chemical gel exhibits a very weak stretch rate dependence, with low λ_C below 2 (Figure 5a). For both dual crosslink gels made from Ni^{2+} and Zn^{2+}, the level of stress increases with $\dot{\lambda}$ as for the unnotched samples. However, λ_C is clearly lower than for unnotched samples and, for the Zn^{2+} gel, λ_C increases from 2.2 to 4.5 with increasing stretch rate while it is nearly independent of $\dot{\lambda}$ in the corresponding unnotched samples. In similar testing conditions, the chemical gel does not show a clear stretch rate dependence and $\sigma_c < 4$ kPa and $\lambda_c < 2$ respectively (data not shown).

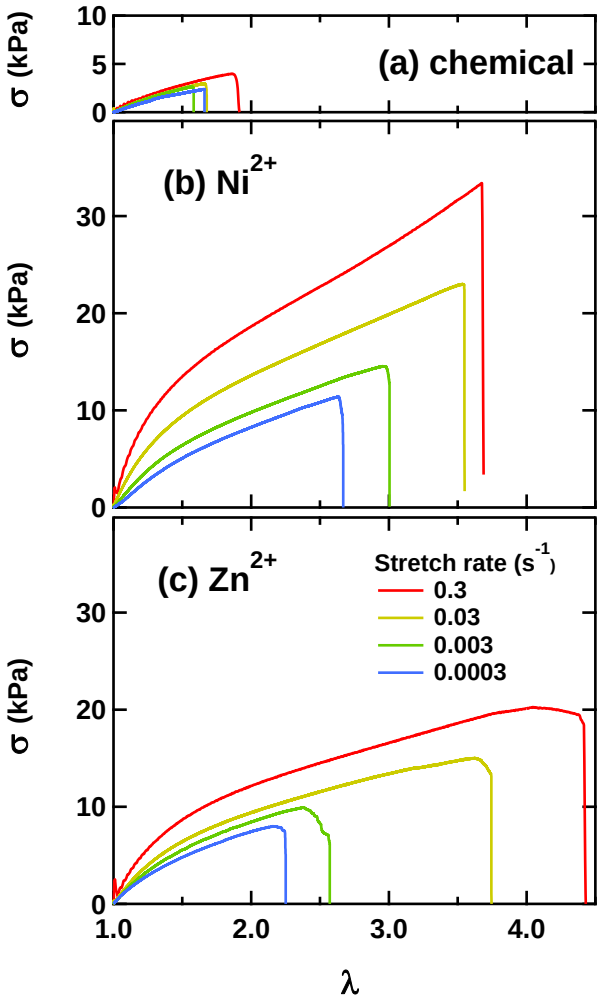

Figure 5. Stress – stretch curves of the notched P(AAm-*co*-VIm)-M^{2+} dual crosslink gels at different stretch rates. (a) Chemical gel, (b) P(AAm-*co*-VIm)-Ni^{2+} dual crosslink gel, (c) P(AAm-*co*-VIm)-Zn^{2+} dual crosslink gel.

It is interesting to examine in **Figure 6**, the values of the initial modulus, $E_{initial}$, for the two dual crosslink gels and for the chemical gel for different values of $\dot{\lambda}$. Qualitatively, $E_{initial}$ is consistent with the linear rheology of **Figure 3**. For the P(AAm-*co*-VIm)-Ni^{2+} gel $E_{initial}$ exhibits a stronger stretch rate dependence than the P(AAm-*co*-VIm)-Zn^{2+} gel or the chemical gel, and the values of $E_{initial}$ for the dual crosslink gels do not reach that of the chemical gel even at the lowest stretch rare studied here. This result can also be explained by the existence of a dilute population of slower transient crosslinks as seen in the linear shear test of **Figure 3**. The same observations have been reported for the stress relaxation in tensile tests (for un-notched samples)[33].

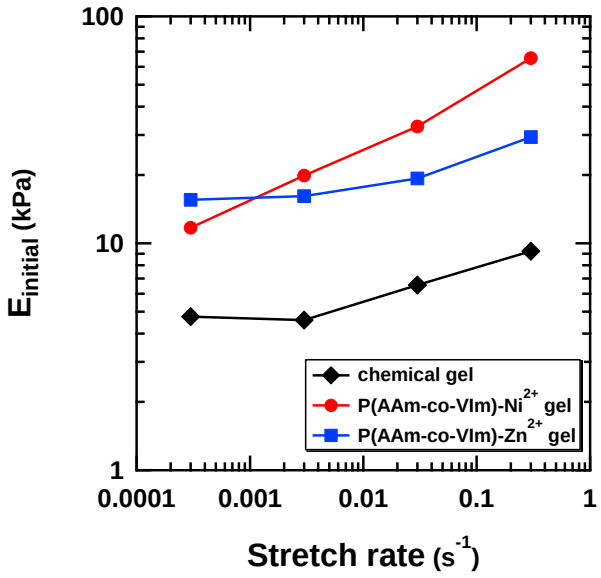

Figure 6. Initial modulus of the chemical gel and two dual crosslink gels with Ni^{2+} and Zn^{2+}, as a function of the stretch rate.

A more characteristic parameter of fracture is the stretch at break λ_C and the values of λ_C are plotted against the stretch rate for both the notched and unnotched P(AAm-*co*-VIm)-M^{2+} dual crosslink gels (**Figure 7**) and the stretch at break of the *un-notched* samples has no clear stretch rate dependence, but does have an ion species dependence. The P(AAm-*co*-VIm)-Zn^{2+} gels

break at $\lambda_C \sim 9$ while the P(AAm-*co*-VIm)-Ni^{2+} gels fail at $\lambda_C \sim 7$ except for $\dot{\lambda} = 0.3\ s^{-1}$. Note that the un-notched chemical gel fails at $\lambda_C \sim 4.6$ at $0.03\ s^{-1}$ -data not shown in the figure).

For *notched* samples on the other hand, we observe no dependence on the ion species, but a stretch rate dependence with λ_C increasing with stretch rate which is actually stronger for the P(AAm-*co*-VIm)-Zn^{2+} gel than for the P(AAm-*co*-VIm)-Ni^{2+} gel unlike the predictions of linear rheology. Furthermore, λ_C is significantly lower for notched samples then for unnotched ones in all cases. This difference between notched and unnotched samples suggests that at the studied condition, flaw-sensitive rupture occurs[39]. In order to evaluate the flaw sensitivity, it is necessary to compare the fracture energy and the work of rupture. We discuss this aspect later in this article.

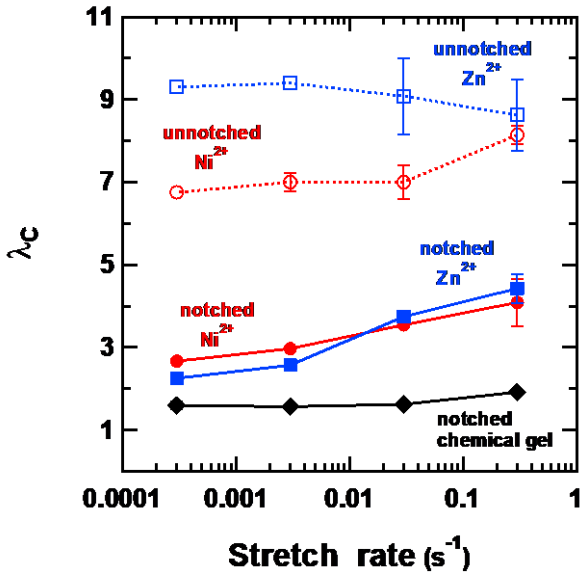

Figure 7. Stretch rate dependence of critical stretch ratio λ_C, for un-notched (filled symbols with a solid line) and notched (open symbols with a dashed line) dual crosslink gels with Ni^{2+} (red circles) and Zn^{2+} (blue squares).

3.3 Crack initiation and propagation processes

Figure 8 shows a typical stress-stretch curve and corresponding images of the propagation of the crack in a notched sample of a P(AAm-*co*-VIm)-Ni^{2+} dual crosslink gel at a stretch rate of

0.03 s^{-1} as example. With increasing stretch λ, the notch starts to gradually open without visible propagation (pictures (a) – (c)) and the radius of the opening continues to increase, very far from a sharp crack. Then close to the critical stretch, the morphology of the crack starts to change (picture (d)), the crack propagates rapidly and the stress σ decreases to zero while the increase of λ measured by the extensometer is very small (pictures (d) – (e)).

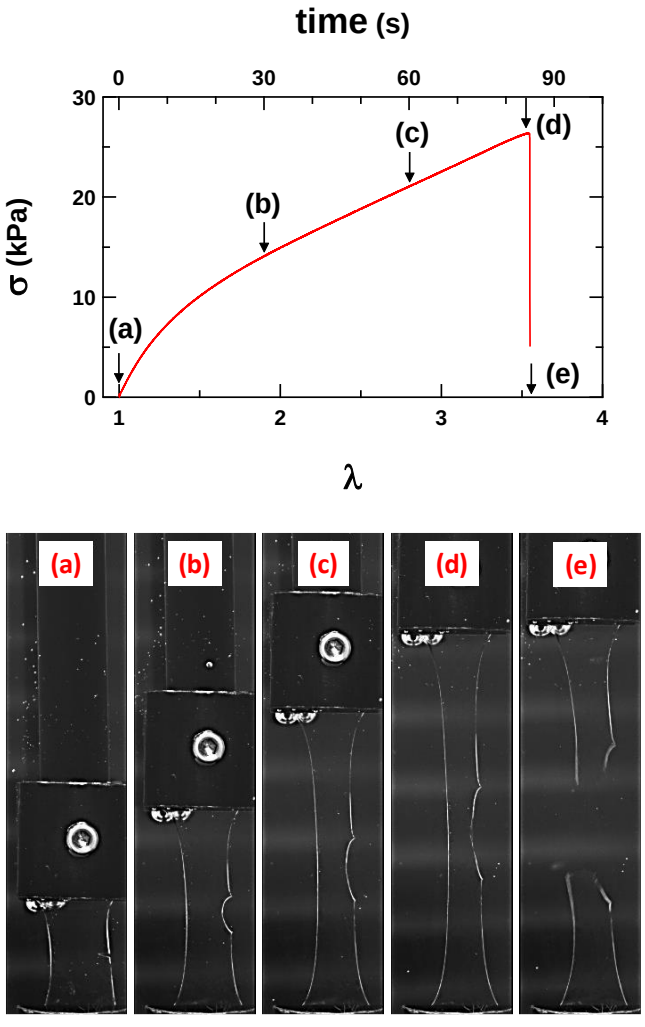

Figure 8. Stress-strain curve of the notched dual crosslink gel at a stretch rate of 0.03 s^{-1}. Corresponding pictures of the gel sample under stretching.

The images of the fracture process synchronized with the stretch-strain curve can be used to estimate the crack propagation velocity and hence the local strain rate near the crack tip[40]. **Figure 9** shows a zoom on the tensile curve at the point where the force drops and the crack propagation becomes fast and four consecutive frames (frame rate: 30 images per second) taken

just before the total rupture of the sample. In the very narrow range in λ, around the maximum value of σ around 26.3 kPa, fibrils are formed at the crack tip of the opened initial notch, while the crack does not propagate. In the pictures (i) and (ii), an extended fibrillary zone is seen. With further increase in λ (and in time), the fibrils break and a new pointier crack opens at the tip of the widely open initial notch (pictures (iii) – (iv)). This process is very fast and the stress decreases very rapidly. The same behavior was found for the same gel stretched at different stretch rates.

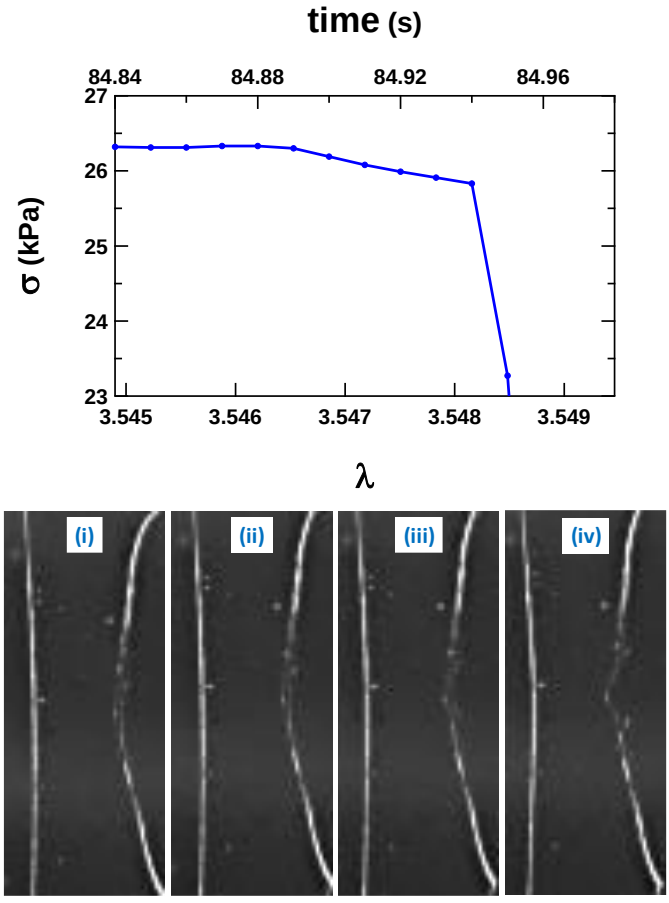

Figure 9. (Graph) Zoomed-in stress-strain curve of the notched dual crosslink gel at the beginning of the crack propagation phase. (Pictures) Four consecutive frames just before the rupture of the sample, showing the sharper tip of the propagating crack (iv).

As previously proposed[9], we estimated the average crack propagation velocity V_P for the stress-stretch curve as $V_P = (w - c)/\Delta t$, where w is the total width of the sample, c is the initial notch

length, and Δt is the duration of the crack propagation period defined as the time interval between the stress maximum and the null stress at complete rupture.

During steady-state crack propagation in elastomers and gels there is usually a unique relation between the driving force (applied energy release rate $\mathcal{G}$) and the crack velocity V_P[41] and **Figure 10** shows V_P as a function of $\dot{\lambda}$ for the two P(AAm-*co*-VIm)-M^{2+} dual crosslink gels and the chemical gel. For the chemical gel, the crack propagation velocity is high and weakly rate dependent. The slight rate dependence is presumably due to the crosslinking ratio, very close to the percolation/gelation limit, thus probably introducing imperfections in its crosslinking structure that can cause a rate dependent dissipation. Fibril formation was not observed. On the other hand V_P exhibits a strong and different power-law dependence on $\dot{\lambda}$ for the P(AAm-*co*-VIm)-M^{2+} dual crosslink gels. For P(AAm-*co*-VIm)-Ni^{2+} $V_P \sim \dot{\lambda}^{1.2}$ while for the P(AAm-*co*-VIm)-Zn^{2+} gel $V_P \sim \dot{\lambda}^{0.56}$.

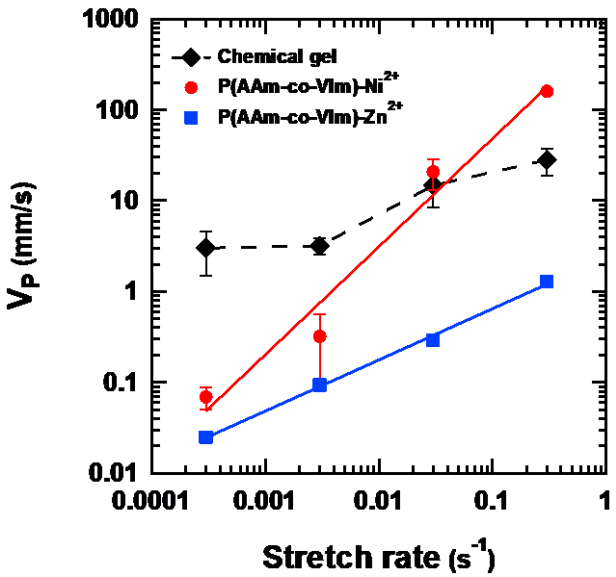

Figure 10. Crack propagation velocity as a function of stretch rate, for the dual crosslink gels and chemical gel. Solid lines are power law fit with an exponent of 1.2 (Ni^{2+}) and 0.56 (Zn^{2+}).

3.4 Fracture energy

To complete the characterization of the crack propagation process we need to quantify the fracture energy Γ of the different materials at different applied stretch rates. The Greensmith approximation is a reasonable starting point for the fracture of soft elastic solids[42]. Briefly, the energy release rate $\mathcal{G}$ of a single edge notch sample of an elastomer can be estimated as

$$\mathcal{G} = 2\frac{3}{\sqrt{\lambda}} c W_{\mathrm{un}}(\lambda) \tag{1}$$

where c is the initial length of the notch, $W_{un}(\lambda)$ is the stored energy density calculated from the uniaxial stress-strain curve of the *un*-notched sample. When $\lambda = \lambda_C$, the crack starts to propagate $\mathcal{G} = \Gamma$, and $W_{\mathrm{un}}(\lambda)$ can be estimated from the area under the stress-strain curve of the *un*-notched sample up to λ_C:

$$W_{\mathrm{un}}(\lambda_C) = \int_1^{\lambda_c} \sigma d\lambda. \tag{2}$$

It is necessary to mention that the estimate of $W(\lambda_C)$ by the Greensmith approximation is only accurate for purely elastic materials at medium strains[43], although it also has been used for viscoelastic materials due to the lack of a better model[8, 44-45]. For elastic materials, the loading and unloading curves are identical, independent of the loading and unloading rates, therefore all the area under loading (unloading) curve is available for fracture. While for viscoelastic materials such as the dual crosslink gels studied in this article, part of the work done upon loading is not elastically stored but already dissipated during loading, leading to an inaccurate estimation of $W_{\mathrm{un}}(\lambda_C)$ by eq.(2)[40].

We previously proposed for the PVA-borax dual crosslink gel[9] an approximate method to separate the energy dissipated before crack propagation from that dissipated during crack propagation and to estimate an "effective" fracture energy, Γ_{local}. The effective energy available for crack propagation should be determined by the area under the unloading curve. In other words, $W_{\mathrm{un}}(\lambda_C)$ determined by eq.(2) overestimates the fracture energy by energy corresponding to the area of the hysteresis loop between loading and unloading curves, which

is dissipated during loading and unavailable for the propagation of the crack as shown schematically in **Figure 11a**.

To apply this method quantitatively, it is necessary to have an unloading curve starting from $\lambda = \lambda_C$, with an unloading rate that is different from the loading rate. Such unloading curve cannot be easily directly measured, thus we make the following two strong assumptions to estimate the hysteresis and the unloading rate from available experimental data. First, we suppose that the unloading rate $\dot{\lambda}_U$ is proportional to crack propagation velocity V_P. It can be estimated with experimentally measureable variables as:

$$\dot{\lambda}_U = \frac{\lambda_C - 1}{\Delta t} = \frac{\lambda_C - 1}{w - c} V_P \tag{4}$$

where Δt is the time necessary for the crack to propagate through the entire sample, w is width of the sample, and c is the initial length of the notch. Second, we suppose that the hysteresis depends on the ion species and on time, but not on the stretch, because of the separability of stretch and time effects. To demonstrate that the second assumption is reasonable, two series of loading/unloading cyclic tests were performed: one series up to a constant maximal stretch of $\lambda_{max} = 2$ at varied stretch rates $\dot{\lambda}$, and the other at a constant stretch rate of $\dot{\lambda} = 0.3\ s^{-1}$ with a variable λ_{max}. The stress-stretch curves for these cycles were previously reported [33]. **Figure 11b** shows the ratio between the hysteresis (hys) and the total energy $W_{un}(\lambda_C)$ (as defined in Fig.11a for each cycle) as a function of time calculated as $t = (\lambda_{max} - 1)/\dot{\lambda}$. For the constant maximal stretch series (filled symbols), the ratio decreases with time (or with decreasing stretch rate) with a power-law exponent of -0.14 for Ni^{2+} or -0.21 for Zn^{2+}. The results for the constant stretch rate series (open symbols) superpose on those of constant λ_{max} series, indicating that the separability holds for the hysteresis. For the P(AAm-*co*-VIm)-Ni^{2+} gel at large λ_{max}, superposition is less satisfactory, presumably due to weak residual deformation that was not fully recovered. Within the range of characteristic times probed here, the fraction hys/W_{un} of

the loading energy that is dissipated upon loading is clearly lower for the P(AAm-*co*-VIm)-Zn^{2+} gel than for the P(AAm-*co*-VIm)-Ni^{2+} gel. This implies qualitatively that for the same value of $W(\lambda_C)$ the actual elastic energy available for crack propagation is higher for the Zn^{2+} gel than for the Ni^{2+} gel.

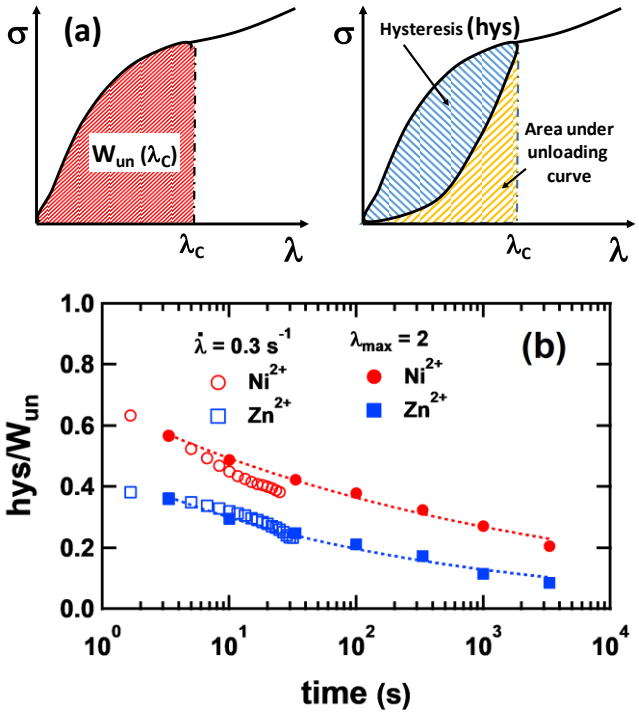

Figure 11. (a) Schematic illustrations to define $W_{un}(\lambda_C)$ and hys. (b) Normalized hysteresis of the P(AAm-*co*-VIm)-M^{2+} dual crosslink gels loading/unloading cycle tests as a function of time. Filled symbols: constant maximal stretch (λ_{max} = 2) with varied stretch rates; open symbols: constant stretch rate ($\dot{\lambda}$ = 0.3 s^{-1}) at varied maximal stretch.

In our previous publication we were able to use a constitutive model to estimate an unloading curve at any unloading rate[9]. Although for the P(AAm-*co*-VIm)-M^{2+} gels the applicability of that model is not confirmed, the value of Γ_{local} at crack propagation can still be roughly estimated from equation 1, by simply replacing G by Γ_{local} on the left-hand side of the equation and replacing $W_{un}(\lambda_C)$ by the area under the unloading curves (as defined in Figure 11a) for a loading unloading cycles in uniaxial extension carried out at a stretch rate defined by equation 4 (i.e. the approximate rate of unloading during crack propagation). A more detailed discussion

of the pitfalls of the estimated energy release rate in viscoelastic materials has been recently given by Long and Hui[40].

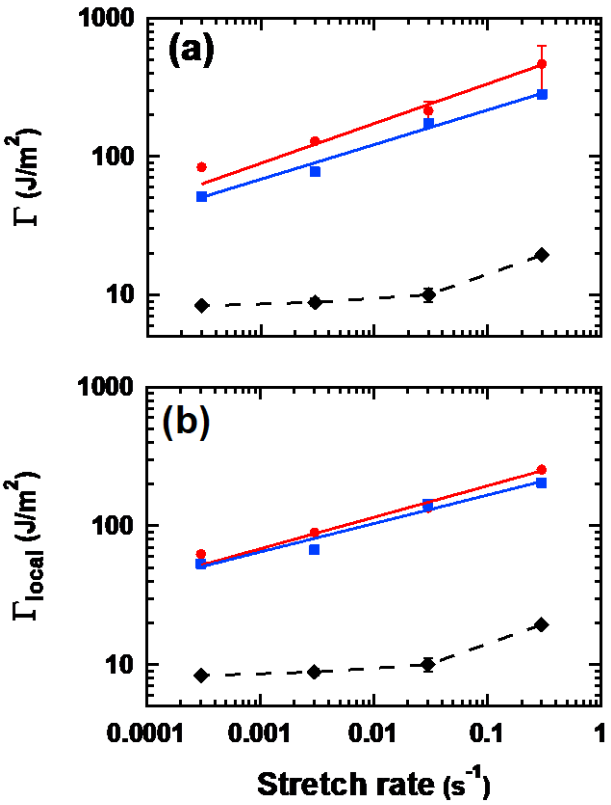

Figure 12. Fracture energy Γ (a) and effective fracture energy Γ_{local} (b) as a function of stretch rate, for chemical gels and dual crosslink gels. Red circles: P(AAm-*co*-VIm)-Ni^{2+} gel, blue squares: P(AAm-*co*-VIm)-Zn^{2+} gel, black diamonds: chemical gel.

Values of the fracture energy Γ (**Figure 12a**) and effective fracture energy Γ_{local} (**Figure 12b**) are plotted for the two dual crosslink gels and for the chemical gel. For both gels $\Gamma > \Gamma_{local}$ and $\Gamma_{local} \sim \dot{\lambda}^{0.22}$ but values of Γ_{local} are nearly the same for both gels while the values of Γ are different.

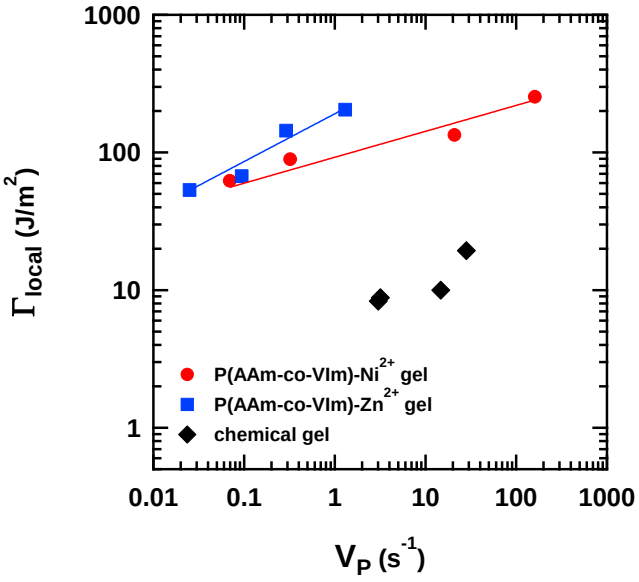

Figure 13. Γ_{local} as a function of crack propagation velocity V_P for the two dual crosslink gels and chemical gel.

Finally, we can address the classic relationship between fracture energy Γ and crack velocity *v*. For viscoelastic solids one can generally write the empirical relation[46]

$$\Gamma(v) = \Gamma_0[1 + \phi(a_T \cdot v)], \quad (3)$$

where Γ_0 is a rate independent threshold value and $\phi(a_T \cdot v)$ is a velocity dependent dissipative factor. Although the functional form may vary from system to system $\phi(a_T \cdot v)$ at a fixed temperature can generally be written as a power-law $\phi(v) \sim v^n$.[47-50] The value of the exponent *n* has been reported to vary between 0.1 and 1 depending on the dissipative nature of the material and low values correspond typically to very elastic materials[51] while high values imply strong viscoelasticity[52]. Our data can be analyzed in this way and **Figure 13** shows the relation between the applied Γ_{local} and V_p. Interestingly and somewhat counterintuitively $n = 0.19$ for the P(AAm-*co*-VIm)-Ni^{2+} gel and $n = 0.35$ For the P(AAm-*co*-VIm)-Zn^{2+} gel. This reflects the fact that the Ni^{2+} based gel mostly dissipates energy upon loading while the Zn^{2+} dissipates most of the energy during propagation, pointing also to the fact that relevant strain rates for fracture are higher at the crack tip than the macroscopically applied stretch rates. The result for the

chemical gel is also shown in the figure, although the range of both Γ and V_P is too small to be quantitatively analyzed.

4. Discussion

4.1 Dissipative zone size and notch sensitivity

As recently point out by Long et al. fracture of elastic soft materials with a rate independent dissipation mechanism, can be described by two length scales, the elasto-adhesive length $\ell = \frac{\Gamma}{E}$ defining the large strain region and the fractocohesive length $\xi = \frac{\Gamma}{W_{un}(\lambda_C)}$ defining the dissipative region at the crack tip. Yet in soft materials with a rate dependent dissipation such as the gels reported here these length scales are ill-defined and in any case depend on strain rate. Nevertheless, for interested readers, we have calculated these lengths scales and they are reported in the Appendix. $\ell \sim 4 - 5$ mm while ξ is of the order of a mm in line with typical tough gels.

Yet the different rate dependence of λ_C for notched and unnotched samples shown in **Figure 7** reveals differences in the value of ξ, i.e. the dissipative zone size with stretch rate as shown in **Figure 14**.

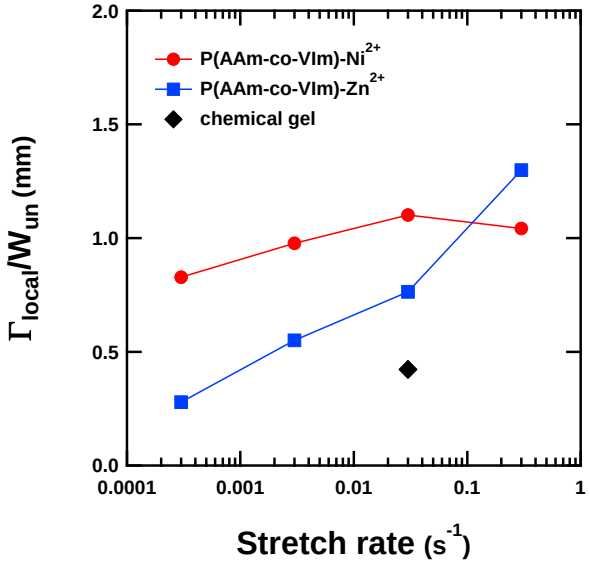

Figure 14. Size of the dissipative zone Γ_{local}/W_{un} of P(AAm-*co*-VIm)-M^{2+} dual crosslink gels and chemical gel as a function of stretch rate.

This implies that when the crack propagates in P(AAm-*co*-VIm)-Zn^{2+} the size of the dissipative zone increases with the applied stretch rate. However, for P(AAm-*co*-VIm)-Ni^{2+} the size of the zone stays constant but the energy dissipated per unit volume increases.

4.2 Comparison between the P(AAm-*co*-VIm)-M^{2+} and the PVA-borax dual crosslink gels

One of the motivations of this study (see introduction) was the possibility to keep the general architecture of dual crosslink gels identical (a low concentration of covalent bonds and a high concentration of dynamic bonds), while varying the characteristic relaxation time. It is, therefore, interesting to compare the fracture properties of the P(AAm-*co*-VIm)-M^{2+} dual crosslink gels with those of the previously investigated PVA-borax dual crosslink gel[9]. Both dual crosslink gel types were designed with the same physical model in mind but with very different relaxation spectrums: at 25 °C, the relaxation times τ_R of these three gels (defined by the peak of $G''(\omega)$) are 1.6 s (PVA-borax), 0.022 s (P(AAm-*co*-VIm)-Ni^{2+}) and 0.00002 s (P(AAm-*co*-VIm)-Zn^{2+}), respectively. Thus in order to compare them and possibly identify a universal behavior, we use the stretch rate normalized by the relaxation time, $\dot{\lambda}\tau_R$.

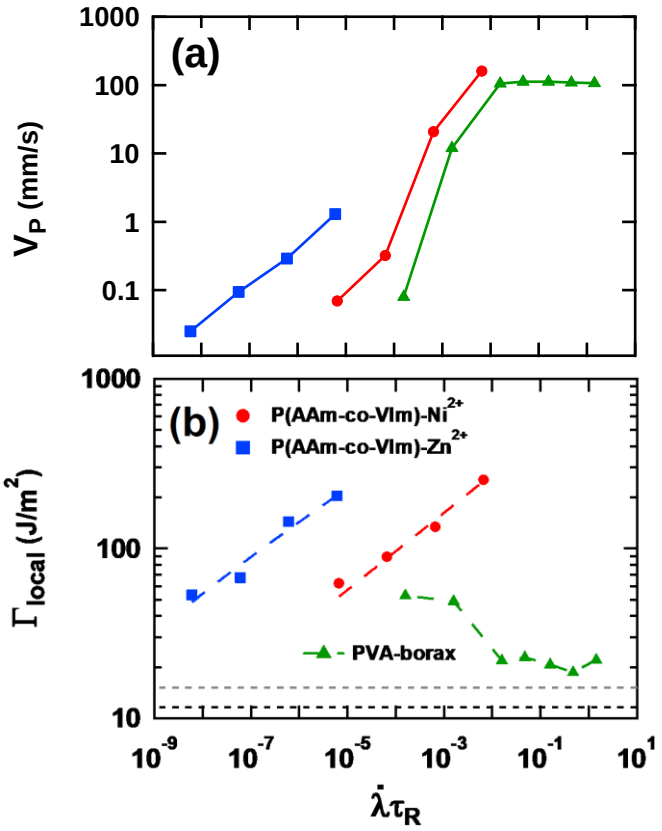

Figure 15. (a) Crack propagation velocity V_P and (b) effective fracture energy Γ_{local}, as a function of the stretch rate normalized by the relaxation time, $\dot{\lambda}\tau_R$, for P(AAm-*co*-VIm)-Ni^{2+} (red circles), P(AAm-*co*-VIm)-Zn^{2+} (blue squares), and PVA-borax (green triangles) dual crosslink gels. Average values of Γ_{local} for the chemical gels are shown as dashed lines (black: P(AAm-co-VIm), gray: PVA).

Figure 15 shows the values of V_P and Γ_{local} as a function of $\dot{\lambda}\tau_R$. It is immediately clear that while there are some obvious trends, there is no universal behavior. For all values of $\dot{\lambda}\tau_R$ except the highest values of $\dot{\lambda}\tau_R$ of the PVA-Borax gel, the effective fracture energy driving the crack Γ_{local} is well above the fracture energy of the chemical gel. Hence very fast exchanging bonds relative to the inverse of the stretch rate are able to effectively increase the stretchability and hence toughen the gel. Then comparing the PVA-borax gel and the two P(AAm-*co*-VIm)-M^{2+} suggests a qualitatively different behavior. For $\dot{\lambda}\tau_R > 10^{-2}$, the value of Γ_{local} of the PVA-borax dual crosslink gel is very close to that of the PVA chemical gel (about 10 – 20 J/m^2, data not shown). As expected by the model[9, 21], at high stretch rates the reversible bonds behave similarly to permanent bonds and the network becomes brittle; thus the fracture energy

decreases. For $\dot{\lambda}\tau_R < 10^{-3}$, the value of Γ_{local} of the PVA-borax gel increases and its $\dot{\lambda}\tau_R$ dependence differs qualitatively from that of the P(AAm-*co*-VIm)-Ni^{2+} gel in the same range in $\dot{\lambda}\tau_R$. For both P(AAm-*co*-VIm)-M^{+} gels, both V_P and Γ_{local} increase continuously with $\dot{\lambda}\tau_R$ although with a very different power-law. Finally, the lack of superposition of P(AAm-*co*-VIm)-Ni^{2+} and P(AAm-*co*-VIm)-Zn^{2+} suggests that the characteristic time found in linear rheology may not be the dominant characteristic time for the fracture behavior.

4.3 Molecular mechanisms

As pointed out above the comparison between the two types of dual crosslink gels points to clear shortcomings in the simple molecular picture of a dual crosslink gel as a combination of independent permanent and dynamic bonds. While this picture seems to hold well for the PVA-borax gel and is consistent with results on linear rheology[20], large strain[21] and fracture[9, 30], our results show that it must be refined for P(AAm-*co*-VIm)-M^{2+} gels.

An important result requiring a discussion for both types of gels is why values of Γ_{local} at low $\dot{\lambda}\tau_R$ never reach the value of Γ_{local} for the chemical gel. While the results on the PVA-Borax gels can be rationalized by arguing that $\dot{\lambda}\tau_R$ is not low enough, this is clearly not possible for P(AAm-*co*-VIm)-Zn^{2+} gels where we report results at much lower values of $\dot{\lambda}\tau_R$.

The high stretchability of the fast exchanging P(AAm-*co*-VIm)-Zn^{2+} dual crosslink gel, even for very low $\dot{\lambda}\tau_R$, suggests that while dynamic bonds have plenty of time to exchange invisibly during the (slow) loading process, they remain present and can delay the correlated scission of neighboring chemical bonds that would lead to the nucleation and growth of a crack. In other words the characteristic time of molecular fracture must be much faster than that of loading and as suggested by Tito et al[35], the presence of dynamic bonds close to the permanent bond may prevent the force transfer from one chemical bond to the next. This result, confirming an earlier result of Craig and coworkers on organogels[32], has important practical relevance since it implies

that fast exchanging bonds can be mechanically invisible during loading/unloading cycles (and hence avoid unwanted energy dissipation in normal usage) while still actively protecting the material from macroscopic fracture.

The other important result begging for a revised molecular picture is the high $\dot{\lambda}\tau_R$ behavior of the Ni^{2+} based gels. Unlike the PVA-Borax gels there are no signs that the P(AAm-*co*-VIm)-Ni^{2+} gels will become brittle at high $\dot{\lambda}\tau_R$. In other words, the dynamic bonds do not behave at the crack tip in the same way as permanent bonds and the gel does not behave like an overcrosslinked brittle network. This is a more difficult question to address and we lack direct molecular information on bond scission. However, we can propose two ideas that may be relevant: The strain rate-dependent strain hardening observed in large strain for P(AAm-*co*-VIm)-Ni^{2+} gels (Figure 4) suggests the existence of a small concentration of longer lived dynamic crosslinks that introduce a second characteristic time, which may be due to the existence of clusters of bonds. Such bonds remain weaker than covalent bonds and within the range of strain rates investigated here become only active as dissipative mechanisms, at the crack tip where strains and stresses are much higher and can accelerate the dynamics of bond scission. The potential toughening effect of such a mechanism, where two populations of dynamic bonds are made dynamic by high stresses only at the crack tip has been discussed theoretically by Hui and coworkers[53]. Slow dynamic bonds that can only dissociate at the crack tip may introduce a strain dependent dissipation mechanism similar to that occurring in double network gels made entirely from covalent bonds[7], which would remain active at the crack tip even at very high strain rates.

5. Conclusion

A series of systematic fracture experiments on P(AAm-*co*-VIm)-M^{2+} dual crosslink gels in a single edge notch geometry were carried out with Ni^{2+} and Zn^{2+} used to create coordination bonds with vinylimidazole. The three key properties characterizing the fracture behavior: stretch at break λ_C, fracture energy Γ and crack propagation velocity V_P, were measured over a wide range of stretch rates for two different ion species (Ni^{2+} and Zn^{2+}) with different characteristic times of transient crosslink dissociation and chain relaxation.

For both dual crosslink gels we found a marked stretch rate dependence of all three parameters with a clear increase in fracture energy with increasing stretch rate. By comparing the P(AAm-*co*-VIm)-M^{2+} dual crosslink gels with the PVA-borax dual crosslink gel we found two major differences in behavior. For a more quantitative comparison of the two dual crosslink gel systems, we used the stretch rate normalized by relaxation time, $\dot{\lambda}\tau_R$. When the effective fracture energy is plotted as a function of $\dot{\lambda}\tau_R$, we find that, unlike the PVA-Borax gel, the P(AAm-*co*-VIm)-M^{2+} dual crosslink gels never become as brittle as the chemical gels. Neither at low $\dot{\lambda}\tau_R$ where elastic properties are nearly the same as those of the chemical gel, nor at high frequency, where the elastic modulus is nearly the same as that of the high frequency modulus of linear rheology.

We rationalize this behavior by enriching the molecular picture of dual crosslink gels with two new mechanisms that could be responsible for the observed toughening.

1) Even fast exchanging bonds could prevent or delay force transfer between covalent bonds upon bond scission (always a much faster event) by sharing the load. This mechanism would be effective at very low $\dot{\lambda}\tau_R$, as long as the characteristic time of covalent bond scission and load transfer is faster than the lifetime of the dynamic bonds.

2) Dynamic bonds could also form longer-lived clusters, introducing a second characteristic time able to create a rate dependent strain hardening, which in turn could stabilize and extend the size of the dissipative zone. This mechanism would introduce a strain-dependent energy dissipation, only active at the crack tip and extend the toughening at high $\dot{\lambda}\tau_R$ where the gel behaves as an overcrosslinked material in the bulk.

6. Acknowledgements

Jingwen Zhao has benefitted from a scholarship from the Chinese Scholarship Council. This project has received funding from the *European Research Council (ERC) under the European Union's Horizon 2020 research and innovation program* under grant agreement AdG No 695351.

7. References

1. Flory, P. J.; Rehner, J., Statistical mechanics of cross-linked polymer networks II Swelling. *Journal of Chemical Physics* **1943,** *11* (11), 521-526.
2. Calvert, P., Hydrogels for Soft Machines. *Adv Mater* **2009,** *21* (7), 743-756.
3. Peppas, N. A.; Langer, R., New challenges in biomaterials. *Science* **1994,** *263*, 1715-1720.
4. Bastide, J.; Candau, S.; Leibler, L., Osmotic deswelling of gels by polymer solutions. *Macromolecules* **1980,** *14*, 719-726.
5. Hong, W.; Zhao, X.; Zhou, J.; Suo, Z., A theory of coupled diffusion and large deformation in polymeric gels. *J Mech Phys Solids* **2008,** *56* (5), 1779-1793.
6. Gong, J. P.; Katsuyama, Y.; Kurokawa, T.; Osada, Y., Double-network hydrogels with extremely high mechanical strength. *Adv Mater* **2003,** *15* (14), 1155-1158.
7. Gong, J. P., Why are double network hydrogels so tough? *Soft Matter* **2010,** *6* (12), 2583-2590.
8. Sun, J.-Y.; Zhao, X.; Illeperuma, W. R. K.; Chaudhuri, O.; Oh, K. H.; Mooney, D. J.; Vlassak, J. J.; Suo, Z., Highly stretchable and tough hydrogels. *Nature* **2012,** *489* (7414), 133-136.
9. Mayumi, K.; Guo, J.; Narita, T.; Hui, C. Y.; Creton, C., Fracture of dual crosslink gels with permanent and transient crosslinks. *Extreme Mechanics Letters* **2016,** *6*, 52-59.
10. Haraguchi, K., Nanocomposite hydrogels. *Current Opinion in Solid State and Materials Science* **2007,** *11* (3-4), 47-54.
11. Liu, C.; Morimoto, N.; Jiang, L.; Kawahara, S.; Noritomi, T.; Yokoyama, H.; Mayumi, K.; Ito, K., Tough hydrogels with rapid self-reinforcement. *Science* **2021,** *372* (6546), 1078-1081.
12. Kim, J.; Zhang, G.; Shi, M.; Suo, Z., Fracture, fatigue, and friction of polymers in which entanglements greatly outnumber cross-links. *Science* **2021,** *374* (6564), 212-216.
13. Okumura, Y.; Ito, K., The Polyrotaxane Gel: A Topological Gel by Figure-of-Eight Cross-links. *Adv Mater* **2001,** *13* (7), 485-487.
14. Henderson, K. J.; Zhou, T. C.; Otim, K. J.; Shull, K. R., Ionically Cross-Linked Triblock Copolymer Hydrogels with High Strength. *Macromolecules* **2010,** *43* (14), 6193-6201.
15. Tuncaboylu, D. C.; Sari, M.; Oppermann, W.; Okay, O., Tough and Self-Healing Hydrogels Formed via Hydrophobic Interactions. *Macromolecules* **2011,** *44* (12), 4997-5005.
16. Haque, M. A.; Kurokawa, T.; Gong, J. P., Anisotropic hydrogel based on bilayers: color, strength, toughness, and fatigue resistance. *Soft Matter* **2012,** *8* (31), 8008-8016.
17. Huang, T.; Xu, H. G.; Jiao, K. X.; Zhu, L. P.; Brown, H. R.; Wang, H. L., A novel hydrogel with high mechanical strength: A macromolecular microsphere composite hydrogel. *Adv Mater* **2007,** *19* (12), 1622-+.
18. Zhao, X., Multi-scale multi-mechanism design of tough hydrogels: building dissipation into stretchy networks. *Soft Matter* **2014,** *10* (5), 672-687.
19. Mayumi, K.; Marcellan, A.; Ducouret, G.; Creton, C.; Narita, T., Stress–Strain Relationship of Highly Stretchable Dual Cross-Link Gels: Separability of Strain and Time Effect. *ACS Macro Letters* **2013,** *2* (12), 1065-1068.
20. Narita, T.; Mayumi, K.; Ducouret, G.; Hebraud, P., Viscoelastic Properties of Poly(vinyl alcohol) Hydrogels Having Permanent and Transient Cross-Links Studied by Microrheology, Classical Rheometry, and Dynamic Light Scattering. *Macromolecules* **2013,** *46* (10), 4174-4183.

21. Long, R.; Mayumi, K.; Creton, C.; Narita, T.; Hui, C.-Y., Time Dependent Behavior of a Dual Cross-Link Self-Healing Gel: Theory and Experiments. *Macromolecules* **2014,** *47* (20), 7243-7250.
22. Guo, J.; Long, R.; Mayumi, K.; Hui, C.-Y., Mechanics of a Dual Cross-Link Gel with Dynamic Bonds: Steady State Kinetics and Large Deformation Effects. *Macromolecules* **2016,** *49* (9), 3497-3507.
23. Zhao, J.; Mayumi, K.; Creton, C.; Narita, T., Rheological properties of tough hydrogels based on an associating polymer with permanent and transient crosslinks: Effects of crosslinking density. *J Rheol* **2017,** *61* (6), 1371-1383.
24. Lin, P.; Ma, S.; Wang, X.; Zhou, F., Molecularly Engineered Dual-Crosslinked Hydrogel with Ultrahigh Mechanical Strength, Toughness, and Good Self-Recovery. *Adv Mater* **2015**, 2054-2059.
25. Shao, C.; Wang, M.; Meng, L.; Chang, H.; Wang, B.; Xu, F.; Yang, J.; Wan, P., Mussel-Inspired Cellulose Nanocomposite Tough Hydrogels with Synergistic Self-Healing, Adhesive, and Strain-Sensitive Properties. *Chemistry of Materials* **2018,** *30* (9), 3110-3121.
26. Luo, F.; Sun, T. L.; Nakajima, T.; King, D. R.; Kurokawa, T.; Zhao, Y.; Ihsan, A. B.; Li, X.; Guo, H.; Gong, J. P., Strong and Tough Polyion-Complex Hydrogels from Oppositely Charged Polyelectrolytes: A Comparative Study with Polyampholyte Hydrogels. *Macromolecules* **2016,** *49* (7), 2750-2760.
27. Sun, W.; Xue, B.; Fan, Q.; Tao, R.; Wang, C.; Wang, X.; Li, Y.; Qin, M.; Wang, W.; Chen, B.; Cao, Y., Molecular engineering of metal coordination interactions for strong, tough, and fast-recovery hydrogels. *Science Advances* **2020,** *6* (16), eaaz9531.
28. Lin, J.; Zheng, S. Y.; Xiao, R.; Yin, J.; Wu, Z. L.; Zheng, Q.; Qian, J., Constitutive behaviors of tough physical hydrogels with dynamic metal-coordinated bonds. *J Mech Phys Solids* **2020,** *139*, 103935.
29. Long, R.; Mayumi, K.; Creton, C.; Narita, T.; Hui, C.-Y., Rheology of a dual crosslink self-healing gel: Theory and measurement using parallel-plate torsional rheometry. *Journal of Rheology (1978-present)* **2015,** *59* (3), 643-665.
30. Guo, J.; Liu, M. L.; Zehnder, A. T.; Zhao, J.; Narita, T.; Creton, C.; Hui, C. Y., Fracture mechanics of a self-healing hydrogel with covalent and physical crosslinks: A numerical study. *Journal of Mechanics and Physics of Solids* **2018,** *120*, 79-95.
31. Guo, J.; Liu, M. L.; Zehnder, A. T.; Zhao, J.; Narita, T.; Creton, C.; Hui, C. Y., Time-temperature equivalence in a PVA dual cross-link self-healing hydrogel. *J Rheol* **2018,** *62*, 991.
32. Kean, Z. S.; Hawk, J. L.; Lin, S.; Zhao, X.; Sijbesma, R. P.; Craig, S. L., Increasing the Maximum Achievable Strain of a Covalent Polymer Gel Through the Addition of Mechanically Invisible Cross-Links. *Adv Mater* **2014,** *26*, 6013-6018.
33. Zhao, J.; Narita, T.; Creton, C., Dual Crosslink Hydrogels with Metal-Ligand Coordination Bonds: Tunable Dynamics and Mechanics Under Large Deformation. In *Self-Healing and Self-Recovering Hydrogels*, Springer Berlin Heidelberg: Berlin, Heidelberg, 2020; Vol. 285, pp 1-20.
34. Debertrand, L.; Zhao, J.; Creton, C.; Narita, T., Swelling and Mechanical Properties of Polyacrylamide-Derivative Dual-Crosslink Hydrogels Having Metal–Ligand Coordination Bonds as Transient Crosslinks. *Gels* **2021,** *7* (2), 72.
35. Tito, N. B.; Creton, C.; Storm, C.; Ellenbroek, W. G., Harnessing entropy to enhance toughness in reversibly crosslinked polymer networks. *Soft Matter* **2019,** *15* (10), 2190-2203.
36. Fullenkamp, D. E.; He, L.; Barrett, D. G.; Burghardt, W. R.; Messersmith, P. B., Mussel-Inspired Histidine-Based Transient Network Metal Coordination Hydrogels. *Macromolecules* **2013,** *46* (3), 1167-1174.
37. Priimov, G. U.; Moore, P.; Helm, L.; Merbach, A. E., Kinetic and Mechanistic Studies of Substitution Reactions of Solvated Cobalt(II), Nickel(II), Copper(II) and Zinc(II) Ions with

2,2′:6′,2″-Terpyridine and Several 2,2′:6′,2″-Terpyridine Derivatives. Evidence for the Formation of Intermediates. *BioInorganic Reaction Mechanisms* **2001,** *3* (1), 1-24.
38. Bauman Jr, J. E.; Wang, J. C., Imidazole complexes of nickel (II), copper (II), zinc (II), and silver (I). *Inorg Chem* **1964,** *3* (3), 368-373.
39. Chen, C.; Wang, Z.; Suo, Z., Flaw sensitivity of highly stretchable materials. *Extreme Mechanics Letters* **2017,** *10*, 50-57.
40. Long, R.; Hui, C.-Y., Fracture toughness of hydrogels: measurement and interpretation. *Soft Matter* **2016,** *12* (39), 8069-8086.
41. Creton, C.; Ciccotti, M., Fracture and Adhesion of Soft Materials: a review. *Rep Prog Phys* **2016,** *79* (4), 046601.
42. Greensmith, H. W., Rupture of rubber. X. The change in stored energy on making a small cut in a test piece held in simple extension. *Journal of Applied Polymer Science* **1963,** *7* (3), 993-1002.
43. Liu, Z.; Zakoworotny, M.; Guo, J.; Zehnder, A. T.; Hui, C.-Y., Energy release rate of a single edge cracked specimen subjected to large deformation. *International Journal of Fracture* **2020,** *226* (1), 71-79.
44. Lin, W. C.; Fan, W.; Marcellan, A.; Hourdet, D.; Creton, C., Large Strain and Fracture Properties of Poly (dimethyl acrylamide)/silica Hybrid Hydrogels. *Macromolecules* **2010,** *43*, 2554-2563.
45. Zhang, H.; Chen, Y. J.; Lin, Y. J.; Fang, X. L.; Xu, Y. Z.; Ruan, Y. H.; Weng, W. G., Spiropyran as a Mechanochromic Probe in Dual Cross-Linked Elastomers. *Macromolecules* **2014,** *47* (19), 6783-6790.
46. Maugis, D.; Barquins, M., Fracture Mechanics and the adherence of viscoelastic bodies. *Journal of Physics D: Applied Physics* **1978,** *11*, 1989-2023.
47. Ahn, D.; Shull, K. R., Effects of methylation and neutralization of carboxylated poly(n-butyl acrylate)on the interfacial and bulk contributions to adhesion. *Langmuir* **1998,** *14* (13), 3637-3645.
48. Nase, J.; Ramos, O.; Creton, C.; Lindner, A., Debonding energy of PDMS. *The European Physical Journal E* **2013,** *36* (9), 1-10.
49. Persson, B. N. J.; Albohr, O.; Heinrich, G.; Ueba, H., Crack propagation in rubber-like materials. *Journal of Physics-Condensed Matter* **2005,** *17* (44), R1071-R1142.
50. Persson, B. N. J., A simple model for viscoelastic crack propagation. *The European Physical Journal E* **2021,** *44* (1), 3.
51. Tanaka, Y.; Kuwabara, R.; Na, Y. H.; Kurokawa, T.; Gong, J. P.; Osada, Y., Determination of fracture energy of high strength double network hydrogels. *Journal of Physical Chemistry B* **2005,** *109* (23), 11559-11562.
52. Plazek, D. J.; Gu, G. F.; Stacer, R. G.; Su, L. J.; Vonmeerwall, E. D.; Kelley, F. N., Viscoelastic Dissipation and the Tear Energy of Urethane Cross-Linked Polybutadiene Elastomers. *Journal of Materials Science* **1988,** *23* (4), 1289-1300.
53. Guo, J.; Zehnder, A. T.; Creton, C.; Hui, C.-Y., Time dependent fracture of soft materials: linear versus nonlinear viscoelasticity. *Soft Matter* **2020,** *16* (26), 6163-6179.

8. Appendix

Figure 16 shows the flaw sensitivity diagram for the three gels representing the ratio of W_n/W_{un} as a function of c/ξ. The dashed line is the generic function proposed by Chen et al.[39] The

points for the PVA borax dual crosslink gel are shown in green and the notch size for those experiments is 1 mm. Interestingly for those gels, the fractocohesive length does not show a very strong stretch rate dependence (about 2.9 – 5.1 mm), while W_n/W_{un} obtained from the tensile curves varies significantly because of the strong stretch rate dependent hysteresis[34]. It might be worth to mention that the fracto-cohesive length increases with decreasing stretch rate, then after a peak it starts to *decrease*, presumably joining the trend of the P(AAm-*co*-VIm)-M^{2+} dual crosslink gels. In conclusion, despite being tougher than chemical gels even at low strain rates, the P(AAm-*co*-VIm)-M^{2+} are very notch sensitive at low strain rates where the ratio W_n/W_{un} is very small (see also Figure 7). This marked difference with the PVA-Borax gel suggests also that there are more differences in molecular mechanisms of bond failure at the crack tip between the two systems than what would be suggested by a change in the main relaxation time.

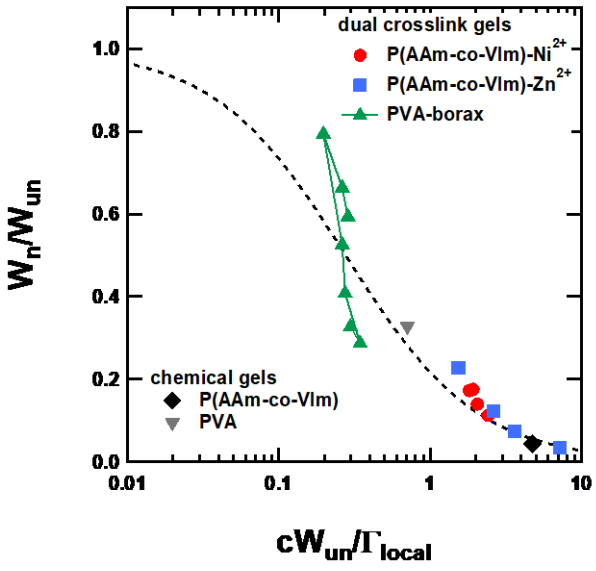

Figure 16. Flaw sensitivity diagram for the three dual crosslink gels and the two corresponding chemical gels. The notch size c ~2 mm for the PVA borax gels for a total width of 10 mm and c ~ 1 mm for the P(AAm-*co*-VIm)-M^{2+} series.